Effects of Unsaturated Moist Froude Number and Orographic Aspect Ratio on a Conditionally Unstable Flow over a Mesoscale Mountain

Shu-Hua CHEN

Department of Land, Air, and Water Resources, University of California, Davis, California, USA
Department of Atmospheric Sciences, National Central University, Chung-I, Taiwan

Yuh-Lang LIN

Department of Physics, North Carolina A&T State University, Greensboro, North Carolina, USA

and

Zhan ZHAO

Department of Land, Air, and Water Resources, University of California, Davis, California, USA

(*Manuscript received 2 July 2007, in final form 7 January 2008*)

Abstract

Idealized numerical simulations of an unsaturated, conditionally unstable flow over a two-dimensional mountain ridge were used to study the effects of the moist Froude number (F_w) and the orographic aspect ratio of mountain height to width (h/a) on the propagation, cloud type, and pattern and amount of rainfall of orographically induced precipitation systems. For low F_w, the flow belonged to an upstream propagating flow regime (i.e., Regime I) and was insensitive to h/a. For large F_w, both F_w and h/a dictated the precipitation pattern and the nature of the convection. When F_w was fixed, the flow shifted toward a downstream propagating regime as h/a increased. This dependence on h/a at higher wind speeds appears to be linked to the advection time and cloud growth time. A slightly larger F_w was required for the regime transition to occur when the fixed aspect ratio was small. We also found that although the local maximum rainfall was not directly controlled by F_w, the total domain rainfall was sensitive to F_w, in particular for Regimes I and II (i.e., flow with a long-lasting orographic convective system over the mountain peak, upslope or lee slope) when the mountain half-width was fixed. On the other hand, for the unstable flow studied here, the total domain accumulated rainfall was not sensitive to h/a when F_w was fixed.

It is suggested that flash floods may occur when quasi-stationary convective precipitation systems stay over the mountain area for flow Regime II or when abundant moisture is supplied for a significant period of time due to a low-level jet for flow Regimes III and IV, which are defined as flow with an orographic convective precipitation system over the mountain and a downstream propagating convective system and flow with an orographic stratiform precipitation system over the mountain and possibly a downstream propagating cloud system, respectively. In addition, local orographic rainfall from stratiform precipitation systems (i.e., Regime IV) can be as heavy as that from convective or mixed type precipitation systems belonging to Regime III.

Corresponding author: Shu-Hua Chen, Department of Land, Air, and Water Resources, University of California, One Shields Avenue, Davis, CA 95616, USA.
E-mail: shachen@ucdavis.edu

1. Introduction

It has been well documented that several flow parameters, such as the wind speed, temperature stratification, convective available potential energy

(CAPE), and the vertical distribution of moisture of the incoming airstream, as well as the mountain geometry dictate the nature of orographically induced convective systems (Smith 1979). Small changes in these control parameters can alter the precipitation distribution and the magnitude of localized maxima. This makes quantitative precipitation forecasting for orographically enhanced precipitation systems especially difficult. Therefore, an understanding of how changes to these control parameters affect orographic precipitation is necessary.

In their idealized simulations of conditionally unstable flow impinging on a two-dimensional, mesoscale mountain, Chu and Lin (2000) noted that the precipitation distribution and propagation of orographically induced cloud systems varies with moist Froude number ($F_w = U/N_w h$), where U is mean wind, h is the mountain height, and N_w is the moist Brunt-Vaisala frequency given by

$$N_w = \frac{g}{\theta_v}\frac{\partial \theta_v}{\partial z}. \quad (1)$$

In Eq. (1), θ_v is the virtual potential temperature and g is gravity. Based on their simulations, three flow regimes were identified. They are: Regime I: flow with an upstream propagating convective system and density current; Regime II: flow with a long-lasting orographic convective system over the mountain peak, upslope, or lee slope; and Regime III: flow with an orographic convective precipitation system over the mountain and a downstream propagating convective system. These same regimes have been reproduced in idealized, three-dimensional simulations (Jiang 2003; Miglietta and Buzzi 2004; Chen and Lin 2005a).

Chen and Lin (2005a) found that when the CAPE of the impinging airstream is decreased, the flow tends to shift to a higher flow regime. Following this line of reasoning, Chen and Lin (2005b; denoted as CL05 hereafter) investigated the combined effects of F_w and CAPE, identifying four flow regimes in the parameter space of (F_w, CAPE). These include Regimes I–III identified by Chu and Lin (2000) and an additional regime, Regime IV: flow with an orographic stratiform precipitation system over the mountain and possibly a downstream propagating cloud system. In addition, CL05 found that a mixed convective and stratiform precipitation system may be produced over the mountain peak for Regime III.

It is well known that the mountain aspect ratio (h/a) plays an essential role in dictating rainfall patterns along the mountain surface (Smith 1979). For broader mountain ranges, the maximum rainfall tends to be positioned on the upstream side of the mountain (Rauber 1992), while the maximum in precipitation tends to be positioned more toward the mountain peak or lee slope for narrow mountains (Sinclair et al. 1997). Colle (2004) studied the relationship between orographic precipitation distribution and environmental conditions and terrain geometry for a stable airstream impinging on a two-dimensional, idealized mountain. His results show that for a relatively weak mean flow, maximum precipitation is a function of mountain slope. For larger mean wind speeds, a wider and higher barrier produces greater precipitation than a low, narrow barrier of the same aspect ratio. Kirshbaum and Durran (2004) studied the factors that control shallow, cellular, warm-rain convection over a two-dimensional mountain using idealized simulations. They found that the mountain aspect ratio is a control parameter for the development of cellular convection, noting that if the mountain half-width is sufficiently reduced, the advective time scale is smaller than the microphysical time scale and the precipitation maximum is shifted to the lee side of the mountain. However, in Kirshbaum and Durran's study, the upstream impinging flow was stable, as in Colle (2004).

In this study, we investigated the combined effects of the mountain aspect ratio (h/a) and the moist Froude number (F_w) on the formation and propagation of precipitation systems associated with conditionally unstable flow over a two-dimensional, mesoscale mountain by performing a series of idealized numerical experiments using the Weather Research and Forecasting (WRF) model. The model characteristics and experiment design will be described in Section 2. The results will be discussed in Section 3, and concluding remarks are made in Section 4.

2. Model description and experiment design

The Advanced Research WRF model (ARW) version 2.0 (Skamarock et al. 2005; Michalates et al. 2001), which is a compressible, three-dimensional, nonhydrostatic model using terrain following coordinates, was used for all simulations presented herein. The governing equations for ARW are written in flux-form and mass and dry entropy are conserved. In this study, the Runge-Kutta third-

order time scheme was employed and fifth and third order advection schemes were chosen for the horizontal and vertical directions, respectively. An open (radiative) lateral boundary condition was used in the north-south direction, a free-slip condition was used for the lower boundary condition, and a periodic boundary condition was used in the east-west direction. A 5 km deep sponge layer was added to the upper part of the physical domain to reduce artificial wave reflection. There were 1000 grid points in the east-west direction with grid spacing of 1 km. In the vertical direction, the grids were stretched with a total of 51 levels from 1000 hPa at the surface to the model top (about 20 km). The Purdue-Lin microphysics parameterization scheme (Chen and Sun 2002) and turbulent kinetic energy diffusion scheme were activated in all simulations.

The idealized, two-dimensional mountain geometry is given by

$$h_s(x) = \frac{h}{1+[(x-x_o)/a]^2}, \tag{2}$$

Where $h_s(x)$, h, a, and x_o are the terrain height, the mountain peak height (2 km), the mountain half-width, and the location of the center of the mountain, respectively. The mountain was introduced impulsively into the basic flow at the initial time of the simulation. All simulations were integrated for 10 h with a time step of 1 s.

The initial conditions were horizontally homogeneous, as given by the Schlesinger (1978) sounding (Fig. 1). This sounding has a CAPE of 3000 J kg^{-1} and an unsaturated moist Brunt-Vaisala frequency (N_w) of 0.0095 s^{-1}. Note that N_w was estimated from the surface to approximately 3 km. The sounding used in this study is relatively more unstable than is typical. This sounding was chosen in order to have a base case with a CAPE comparable to the sounding used in Chu and Lin (2000) and Chen and Lin (2005a, 2005b) so that the resulting dynamics and flow fields can be compared with these studies more directly.

In order to study the effects of the moist Froude number (F_w) and the aspect ratio (h/a) on the formation and propagation of orographically induced convective systems, a two-dimensional matrix of experiments was devised (Table 1). F_w was varied by changing the basic state wind speed (U). The values of U that were used are 2.5, 5, 7.5, 10, 15, 20 and 30 m s^{-1}, which correspond to F_w of 0.131 (F1 in Table 1), 0.262 (F2), 0.393 (F3), 0.524 (F4), 0.786 (F5), 1.048 (F6), and 1.572 (F7), respectively. In the second dimension of experiments, h/a was varied by setting a to be 7.5, 15, 22.5, 30, and 45 km, which are named A1 to A5 in Table 1. The experiments were combinations between F1-7 and A1-5 (Table 1). In all experiments, h was 2 km.

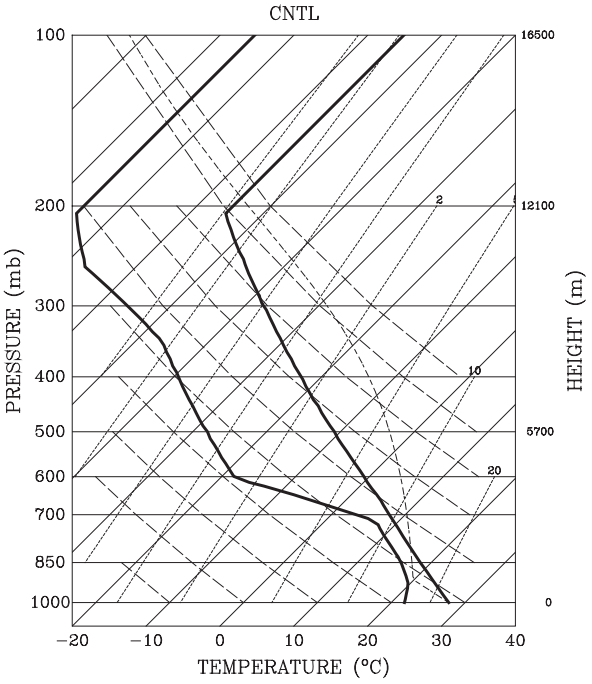

Fig. 1. The sounding used for the initial conditions of numerical experiments. The sounding is identical to that of Schlesinger (1978) and has a CAPE about 3000 J kg^{-1}.

3. Results and Discussion

Figure 2 shows the time evolution of the vertical velocity at 3.6 km height and accumulated rainfall at the surface for four cases with h/a held constant at 2/7.5 (h = 2 km, a = 7.5 km) and F_w = 0.262, 0.524, 0.785, and 1.572. The variation of resulted from varying U = 5, 10, 15, and 30 m s^{-1}. The corresponding vertical cross-sections of the vertical velocity and potential temperature after 7-h simulation are shown in Fig. 3. For the case of F_w = 0.262 (U = 5 m s^{-1}) (Figs. 2a and 3a), the convective system generated by the orographic lifting propagated upstream and can thus be identified as Regime I as defined in CL05. As the F_w increased to 0.524 (U = 10 m s^{-1}) (Figs. 2b and 3b), the upstream propagating convective system

Table 1. The classification of flow regimes with respect to the unsaturated moist Froude number (F_w) and the aspect ratio (h/a). The basic wind speed (U) and the mountain half-width (a) corresponding to each case are identified in the parentheses.

	A1 (h/a = 2/7.5) (a = 7.5 km)	A2 (1/15) (15 km)	A3 (2/22.5) (22.5 km)	A4 (2/30) (30 km)	A5 (2/45) (45 km)
F1 (F_w = 0.131) (U = 2.5 m/s)	I	I	I	I	I
F2 (.262) (5 m/s)	I	I	I	I	I
F3 (0.393) (7.5 m/s)	I	I	I	I	I
F4 (0.524) (10 m/s)	II	I	I	I	I
F5 (0.786) (15 m/s)	III	III	II	II	II
F6 (1.048) (20 m/s)	III	III	III	III	III
F7 (1.572) (30 m/s)	IV	III	III	III	III

became quasi-stationary and situated over the mountain peak. Thus, this flow can be classified as Regime II. The downstream propagating convective system shown in the time evolution figure (Fig. 2) was caused by the startup process of numerical integration. Increasing F_w further to 0.785 (U = 15 m s^{-1}) (Figs. 2c and 3c) resulted in an orographic convective or mixed convective and stratiform precipitation system over the mountain and a downstream propagating convective system. This flow belongs to Regime III. Note that besides having a stronger maximum vertical velocity, a convective cloud develops in a cellular type and its depth varies significantly. In contrast, the depth of a stratiform cloud does not change much and belongs to a stationary type as long as the forcing exists. For a very large moist Froude number (F_w = 1.572; corresponding to U = 30 m s^{-1}) (Figs. 2d and 3d), a stratiform precipitation system was located over the mountain peak (Fig. 3d) and there was a downstream propagating convective system which was advected faster than those in the smaller F_w cases. This large F_w flow is classified as Regime IV.

The results described above show that flow transits to higher number regimes as F_w (i.e., U) increases. This is consistent with previous findings by Chu and Lin (2000) and CL05. The experiments mentioned above also serve as a way to verify the model results. Similar results were also found when varying F_w with a fixed at 15, 22.5, 30, and 45 km, but the critical F_w for flow regime transition became a function of h/a. In other words, a slightly larger F_w was required for the regime transition to occur when the aspect ratio (mountain half-width) became smaller (larger) (i.e., column A1 vs. column A5 in Table 1). For example, flow transition from Regime I to II occurred between U = 10 and 15 m s^{-1} for a = 22.5, 30, and 45 km, while it occurred between U = 7.5 and 10 m s^{-1} for a = 7.5 km. These results are summarized in Table 1. The requirement for stronger winds to transition to a higher number flow regime as a increases can be understood by comparing the advective time scale ($\tau_{adv} \sim a/U$) and the cloud development time scale ($\tau_{cloud} \sim 1000$ s). As a increases (i.e., h/a decreases), τ_{adv} also increases. This implies that convective systems have a longer residence time to develop on the upslope of the mountain. In consequence, a stronger cold pool can be produced to act against the basic-state flow. This further acts to propel the flow to a lower number regime. Therefore, a larger F_w is required in order to shift the flow toward a higher number regime.

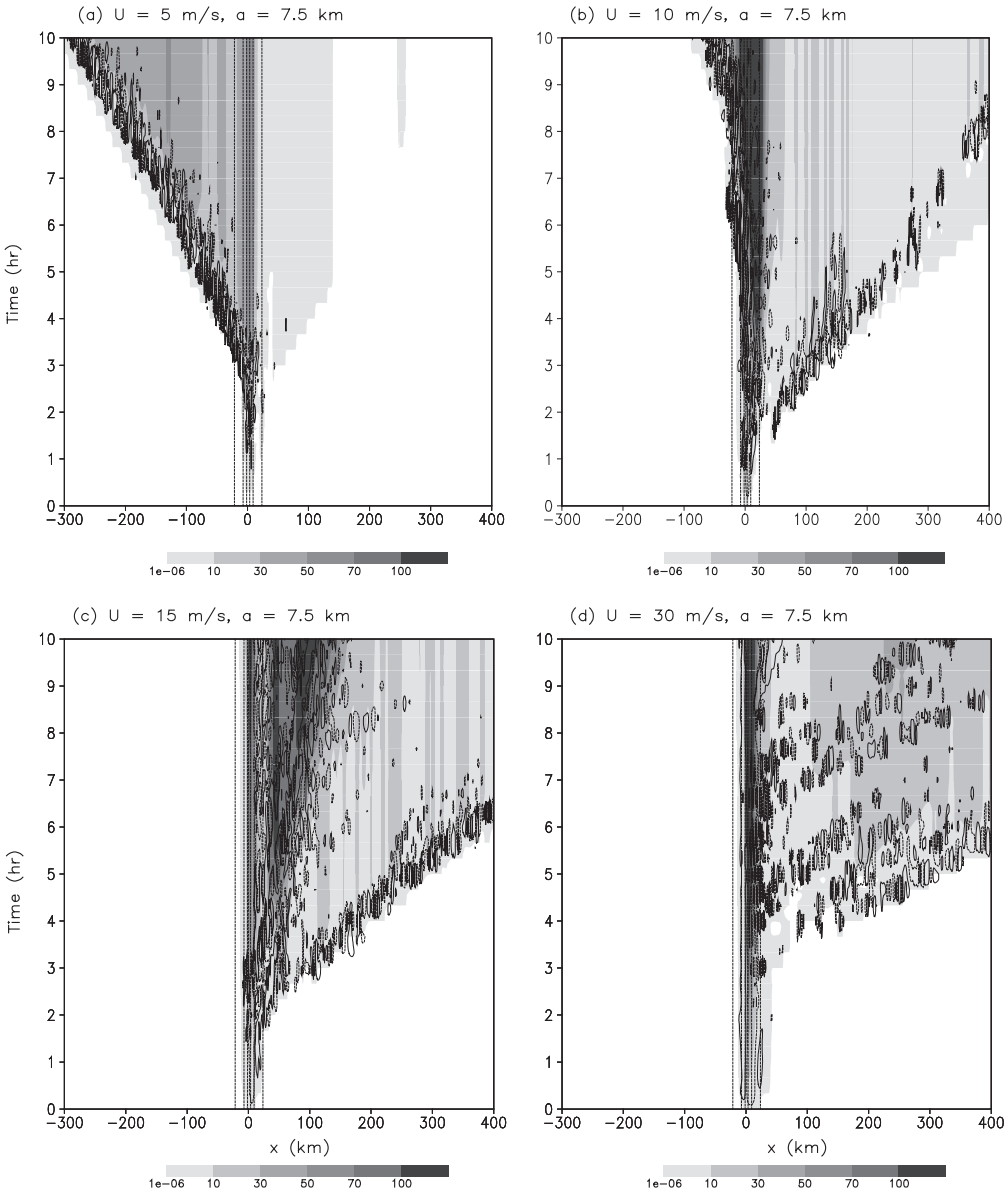

Fig. 2. Time evolution of the vertical velocity at 3.6 km height (dashed contour lines for –2 m s^{-1} and solid contour lines for 2 m s^{-1}) and accumulated rainfall (shaded; mm) for U = (a) 5 m s^{-1}, (b) 10 m s^{-1}, (c) 15 m s^{-1}, and (d) 30 m s^{-1}. The mountain half-width is 7.5 km and the mountain height is 2 km (h/a = 2/7.5). The corresponding F_w are 0.262, 0.524, 0.786, and 1.572, respectively. Dotted lines indicate elevation (200 m, 1000 m, and 1800 m), where the mountain peak is at x = 0 km.

3.1 Dependence of rainfall pattern on moist Froude number

Figure 4a shows the spatial distribution of total accumulated rainfall after 10-h simulations for U = 7.5, 10, 15, 20, and 30 m s^{-1} and a fixed a = 7.5 km (h/a = 2/7.5). The corresponding moist Froude numbers are 0.393, 0.524, 0.786, 1.048, and 1.572. The rainfall distribution varied significantly for different moist Froude numbers (basic wind speeds). With a weaker wind, the rainfall spread farther upstream due to the stronger density current pushing against the weaker basic wind (Fig. 3a). This is consistent with the time evolution of the accumulated rainfall (Fig. 2); the rainfall spread farther upstream for the flow regime with upstream propagating convective systems (Regime

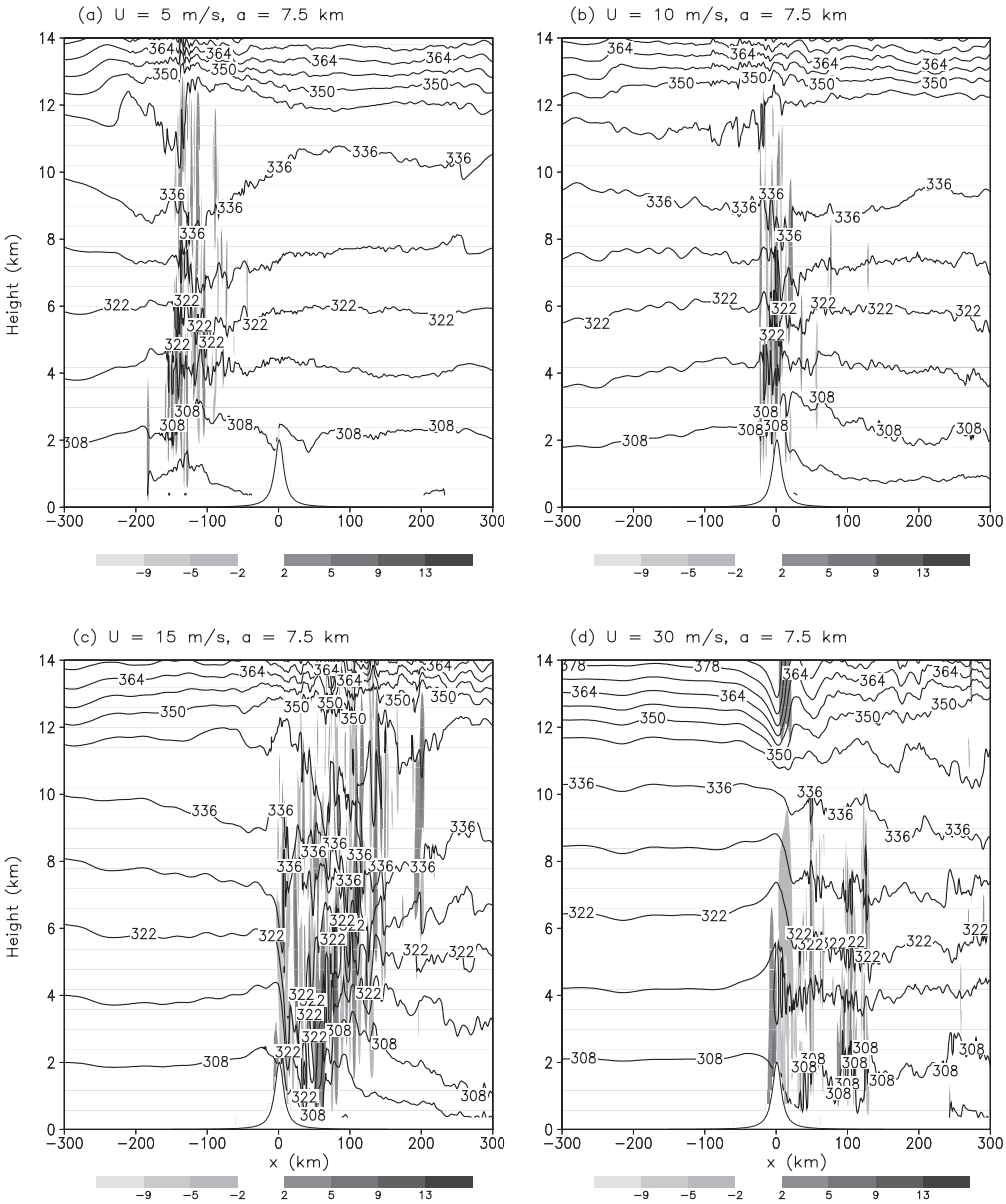

Fig. 3. Vertical cross-section of the vertical velocity (in m s^{-1}; shaded) and potential temperature (solid lines with a contour interval of 7 K) for U = (a) 5 m s^{-1}, (b) 10 m s^{-1}, (c) 15 m s^{-1}, and (d) 30 m s^{-1} after 7-h simulation. The mountain half-width is 7.5 km and the mountain height is 2 km (h/a = 2/7.5). The corresponding F_w are 0.262, 0.524, 0.786, and 1.572, respectively.

I; U = 7.5 m s^{-1}). For the flow regime with stationary convective systems over the mountain (Regime II; U = 10 m s^{-1}), the rainfall was concentrated around the mountain peak and there was more accumulated rainfall than for Regime III (U = 15 and 20 m s^{-1}). The rainfall region over the lee side of the mountain extended farther downstream when U increased due to stronger advection for regimes III (U = 15 and 20 m s^{-1}) and IV (U = 30 m s^{-1}).

For the A1F4 case (a = 7.5 km and U = 10 m s^{-1}; thin-dotted line in Fig. 4a), which is classified as Regime II, extremely heavy local accumulated rainfall (> 200 mm after 10-h simulation) occurred near the top of the lee-side mountain due to long quasi-stationary convective precipitation systems over the region. This heavy precipitation zone over

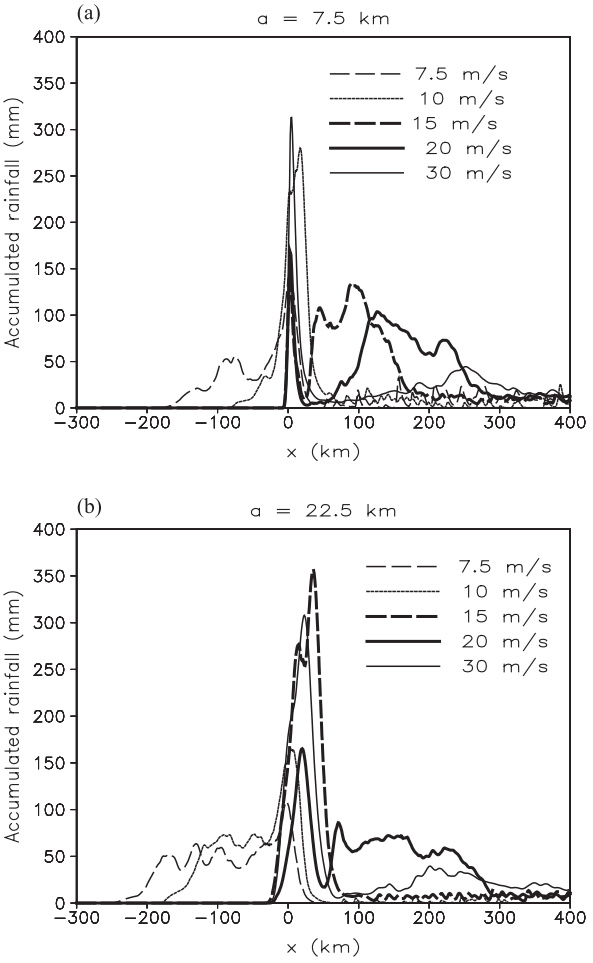

Fig. 4. Spatial distribution of total accumulated rainfall (mm) after 10-h simulations for U = 7.5, 10, 15, 20, and 30 m s^{-1}. The corresponding F_w are 0.393, 0.524, 0.786, 1.048, and 1.572, respectively. The mountain half-width is (a) 7.5 km and (b) 22.5 km. The mountain height is 2 km.

the mountain had a wider distribution than those from other cases with the same half-width (i.e., a = 7.5 km) which is due to the convective systems spreading to a larger area and oscillate around the mountain. Surprisingly, the maximum local accumulated rainfall in the vicinity of the mountain peak for the Regime IV (U = 30 m s^{-1}; A1F7) case was even larger than that for A1F4. For this case, the orographic clouds could not develop into convective clouds due to strong advection by the basic wind (i.e., small τ_{adv}). Although the precipitation cloud systems over the mountain peak for the A1F7 case were stratiform, they were still able to produce heavier rainfall in a very narrow zone (Fig. 4a) because: 1) moisture supply (~ qU) was abundant due to strong basic wind (U = 30 m s^{-1}); 2) unlike cases A1F5 and A1F6, there were no convective systems developed far downstream from the mountain peak, resulting in more moisture supply in the vicinity of the mountain peak; and 3) the stratiform precipitation systems stayed at approximately the same location for a long time period.

The domain integrated accumulated rainfall amounts with respect to different moist Froude numbers (i.e., U) at two hour intervals are plotted in Fig. 5a for a fixed h/a (a = 7.5 km, h = 2 km). For an unstable flow, although the local maximum rainfall was not directly correlated to mean wind (Fig. 4a), the domain integrated rainfall amount increased as the basic wind speed strengthened, except for the case of U = 30 m s^{-1} (F_w = 1.572). The strongest response of rainfall to increasing basic wind speed was seen in flow Regimes I and II. For cases of $U \leq$ 20 m s^{-1} ($F_w \leq$ 1.048), the dynamics can be explained as follows. CL05 demonstrated that when Convective Available Potential Energy (CAPE) increases, flow transits to a lower number flow regime. When the mountain width (a) is fixed, an environment with a larger CAPE is equivalent to one with both a smaller CAPE and a smaller F_w (or a weaker basic wind). This implies that when crossing a mountain, large CAPE flows require a longer advection time than flows with the same basic wind but a smaller CAPE. It is true that a 7.5 km mountain half-width is not large, however, since the CAPE of the environment flow in this study is large (3000 J kg^{-1}), the convective system can develop over the mountain region with a reasonably sized mountain half-width (or with a smaller F_w). In this situation, water vapor supply can dominate the rainfall amount. When the basic wind gets stronger, a greater amount of moisture is transported into the convective region (i.e., qU, where q is the water vapor mixing ratio), and precipitation can be produced more efficiently through microphysical processes. This will not hold true for cases where the basic wind speed is too strong and the mountain half-width is too narrow (e.g., a = 7.5 km and U = 30 m s^{-1} in Fig. 5a; Regime IV). Under these conditions, instead of a deep convective cloud system a stratiform cloud system develops in the vicinity of the mountain ridge (i.e., $\tau_{adv} < \tau_{cloud}$) and the system quickly propagates downstream. The downstream-propa-

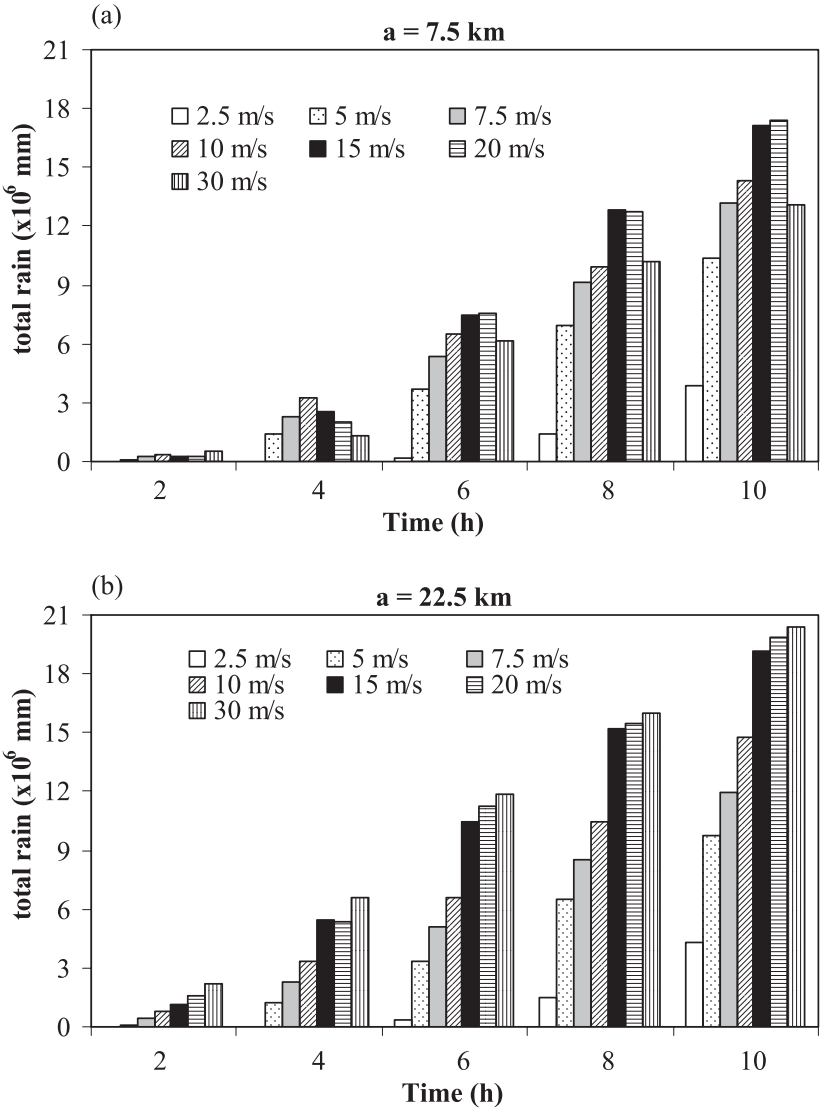

Fig. 5. Accumulated total rainfall (mm) after 2-, 4-, 6-, 8-, and 10-h integration for U = 2.5, 5, 7.5, 10, 15, 20, and 30 m s^{-1}. The mountain half-width is (a) 7.5 km and (b) 22.5 km. The mountain height is 2 km.

gating system may develop into a convective one if environmental conditions are favorable; however, the convective system is relatively weak for the present case (Fig. 3d). Compared with A1F5 and A1F6, although the basic wind is stronger (i.e., larger moisture flux) and the maximum local accumulated rainfall is higher from A1F7 (Fig. 4a), the weak downstream-propagating convective system cannot efficiently produce rainfall. Therefore, the domain integrated rainfall amount is less than those from A1F5 and A1F6.

To further prove this concept, the spatial distributions of total accumulated rainfall after 10-h simulations for U = 7.5, 10, 15, 20, and 30 m s^{-1} for a wider mountain, a = 22.5 km (h/a = 2/22.5), were examined (Fig. 4b). Due to regime transition (to be explained in Section 3.2), the rainfall from A3F3 and A3F4 (U = 7.5 and 10 m s^{-1}; Regime I) spread farther upstream compared with that from A1F3 and A1F4 (a = 7.5 km), respectively, (Fig. 4a) and the maximum rainfall over the mountain peak was reduced. Again, the Regime II case (U = 15 m s^{-1}; A3F5) had its maximum rainfall over the mountain peak due to a quasi-stationary convective precipitation system. For A3F7 (a = 22.5 km and U = 30 m s^{-1}), which is classified as Regime III, heavy

local accumulated rainfall occurred over the mountain peak due to abundant moisture supply by the strong mean flow, but with a more widely spread area than that from A1F7 (Regime IV) whose half-width was smaller. Note that the precipitation systems over the mountain area for A3F7 were mixed types (i.e., interchanging convective and stratiform clouds). Figure 5b shows the domain integrated accumulated rainfall after 2-, 4-, 6-, 8-, and 10-h integration for $U = 2.5$, 5, 7.5, 10, 15, 20, and 30 m s^{-1}. The mountain half-width is 22.5 km and the mountain height is 2 km (h/a=2/22.5). The corresponding moist Froude numbers were 0.131, 0.262, 0.393, 0.524, 0.786, 1.048, and 1.572, respectively. The result is similar to that shown for the narrower mountain ($a = 7.5$ km) cases (Fig. 5a), except that the total rainfall amount increased as the flow transited to higher number regimes, which was again clearest with the lower number flow regimes of I and II.

3.2 *Dependence of flow regimes and rainfall pattern on aspect ratio*

Figure 6 shows the vertical cross sections of the vertical velocity, potential temperature, and cloud fields with $a = 7.5$ km, 22.5 km, and 45 km when a fixed basic wind speed of 7.5 m s^{-1} ($F_w = 0.393$) is used (i.e., cases A1F3, A3F3, and A5F3 as listed in Table 1). Note that cellular convective clouds occurred in all of these cases and propagated upstream. All of these flows are classified as Regime I (see Table 1), based on CL05's regime definitions. When the mountain half-width (aspect ratio) gets larger (smaller), which induces a larger lifting area, the convective system spread more widely over the upslope, and the leading convective cell was located farther upstream (Fig. 6). This explains why the convective system can propagate further upstream and the rainfall can thus spread further upstream (Fig. 7a) when the mountain half-width gets larger. The regime diagram (Table 1) indicates that for low F_w, the flow was insensitive to h/a and was in an upstream propagating flow regime (i.e., Regime I).

Figure 7b shows the domain integrated rainfall after 2-, 4-, 6-, 8-, and 10-h integration for $a = 7.5$, 15, 22.5, 30, and 45 km when $U = 7.5$ m s^{-1} ($F_w = 0.393$) is fixed. One noticeable feature of this figure is that the accumulated total rainfall for all these cases is about the same, even at different times. In other words, for a conditionally unstable flow the total rainfall amount is insensitive to the aspect ratio. In fact, after inspecting other cases (not shown) with smaller fixed moist Froude numbers (e.g., $F_w < 0.524$ or $U < 10$ m s^{-1}), we found that the flow is in an upstream propagating regime (Table 1) and the accumulated total rainfall amount is independent of the aspect ratio (Fig. 7b); but, the rainfall spreads farther upstream for mountains with smaller aspect ratio (wider mountains) (Fig. 7a). This is because the convective system has enough time to develop over the mountain region (i.e., $\tau_{adv} > \tau_{cloud}$), and the advection is too weak to counteract the mountain blocking effect and the cold pool. Nevertheless, the location of the convective system and the distribution of the precipitation can be very different from case to case.

Figures 8a, 8c, and 8e show the vertical velocity and potential temperature after 5-h simulation for mountain half-widths of 7.5, 22.5, and 45 km when $U = 30$ m s^{-1} ($F_w = 1.572$) is held constant. The corresponding total hydrometeor contents for Figs. 8a, 8c, and 8e are shown in Figs. 8b, 8d, and 8f, respectively. As indicated in Table 1, all cases belong to Regime III except that with $a = 7.5$ km, which belongs to Regime IV. As discussed earlier (Figs. 3–4), for the case with very strong basic wind and very narrow mountain, such as when $a = 7.5$ km and $U = 30$ m s^{-1}, instead of a deep convective cloud a stratiform cloud (Fig. 8b) developed near the mountain peak when flow crossed the mountain (i.e., $\tau_{adv} < \tau_{cloud}$) and quickly propagated downstream. With wider mountains ($a = 22.5$ and 45 km, Figs. 8c–f), convective clouds were able to develop to a height of about 7 km and several convective clouds were present in the vicinity of the mountain peak. This provides additional evidence validating the argument that the dominance of flow regimes, rainfall patterns, and accumulated total rainfall amounts depends on the relative magnitudes of timescales between cloud advection and development.

It appears that for large F_w, both F_w and h/a dictate the precipitation pattern and the nature of the convection. The flow shifts toward a downstream propagating regime with the increase of h/a if F_w is fixed (Table 1). This dependence on h/a for larger wind speeds appears to be linked to the competition between advection time and cloud development time. In other words, when flow crosses a mountain range, the advection time becomes smaller when h/a becomes larger.

The spatial distributions of total accumulated rainfall after 10-h simulations for $a = 7.5$, 15, 22.5,

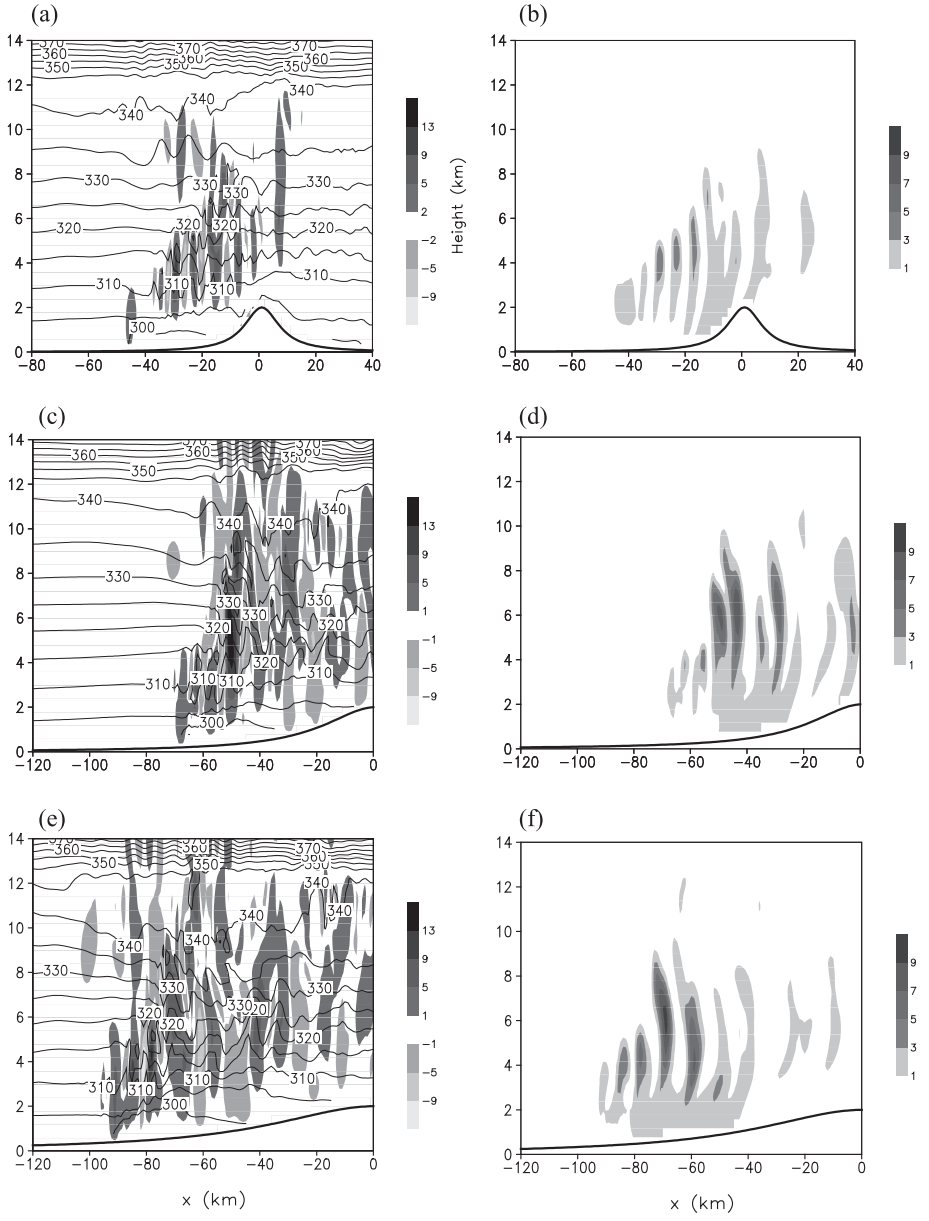

Fig. 6. The vertical velocity (shaded; m s^{-1}) and potential temperature (contour; K) for a = (a) 7.5 km, (c) 22.5 km, and (e) 45 km when U = 7.5 m s = at 5-h simulation. The basic wind speed is 7.5 m s^{-1} and h = 2 km. (b), (d), and (f) are the same as (a), (c), and (e), respectively, except for the cloud fields that include all hydrometeors, (g kg^{-1}). Note that the range of the x-axis differs for (a) and (b).

30, and 45 km and U = 30 m s^{-1} (F_w = 1.572) are shown in Fig. 9a. Due to strong advection by the basic wind, downstream convective systems were unable to develop to intensive ones and little rainfall was produced downstream of the mountain. In addition, the downstream rainfall was spread over a wider region due to strong advection. Therefore, the maximum rainfall areas in these cases were focused in the vicinity of the mountain. Figure 9b shows the domain integrated accumulated total rainfall after 2-, 4-, 6-, 8-, and 10-h integration. The integrated total rainfall amount was almost independent of the aspect ratio after 4-h simulation except that it was smaller for the case of a = 7.5 km.

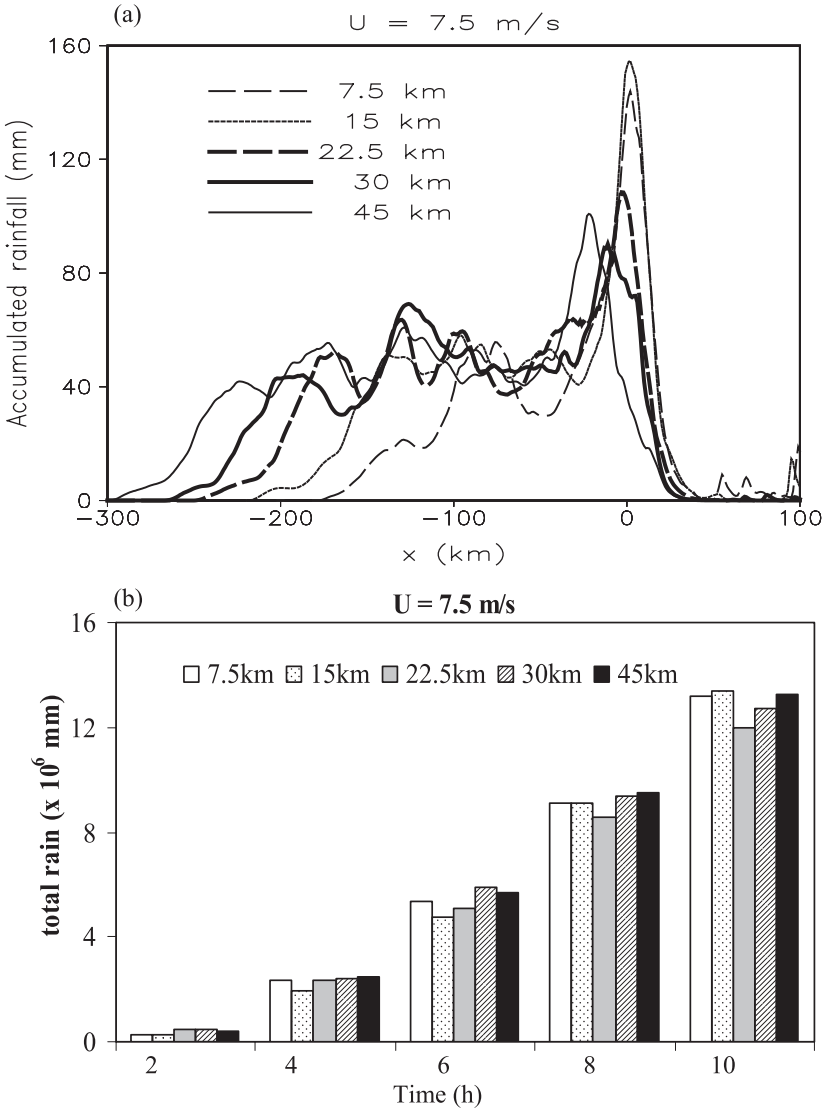

Fig. 7. (a) Spatial distribution of total accumulated rainfall (mm) after 10-h simulations and (b) accumulated total rainfall (mm) after 2-, 4-, 6-, 8-, and 10-h integration for a = 7.5, 15, 22.5, 30 and 45 km when U =7.5 m s^{-1} (F_w = 0.393) and h = 2 km.

3.3 Heavy Local Orographic Rainfall and Flow Regime

We found that heavy local accumulated rainfall (rainfall greater than 200 mm), i.e., a potential for flash flood, over mountainous regions can happen when abundant moisture is supplied for a significant period of time for Regime III (A2-5F7 in Fig. 9a) and even for Regime IV (A1F7 in Fig. 9a), which has a stratiform instead of a convective cloud system over the ridge. The abundant moisture supply can result from strong low-level winds (i.e., a low-level jet) with reasonable moisture content in the atmosphere. It is worth mentioning again that the maximum local accumulated rainfall from a stratiform precipitation system in the vicinity of the mountain (i.e., A1F7, thin-dashed line in Fig. 9a; Regime IV) can be as heavy as that from convective or mixed type systems (i.e., A2F7-A5F7, other lines in Fig. 9a; Regime III). Another source of heavy orographic rainfall (flash flood) is quasi-stationary convective precipitation clouds that stay over the mountain region for a long period of time (e.g., Regime II) as in A1F4 (thin-dotted line in Fig. 4a). This is also demonstrated by other cases

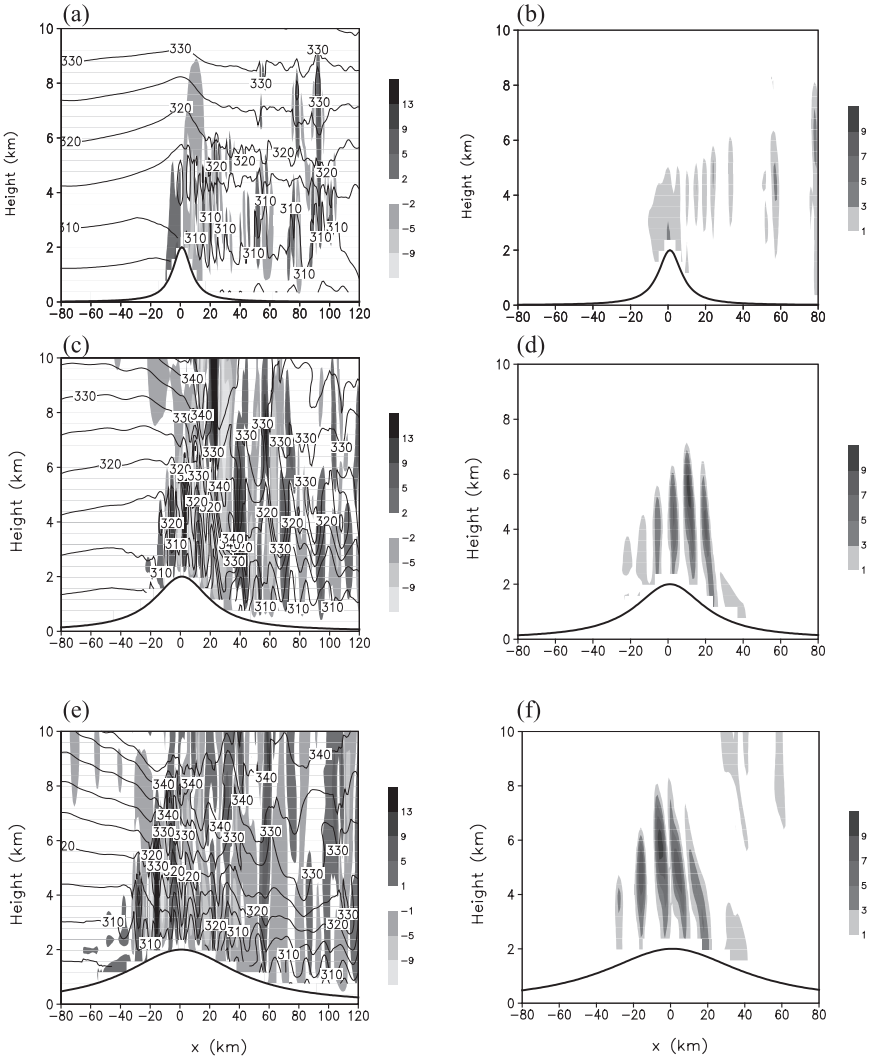

Fig. 8. The vertical velocity (shaded; m s^{-1}) and potential temperature (contour; K) for a = (a) 7.5 km, (c) 22.5 km, and (e) 45 km when U = 30 m s^{-1} (F_w = 1.572) at 5-h simulation. The mountain height is 2 km. The total hydrometeor contents (in g kg^{-1}) for (a), (c), and (e) are shown in (b), (d), and (f), respectively.

whose flows belong to Regime II, as shown in Fig. 10 (i.e., A3-5F5).

4. Conclusions

Idealized simulations for an unsaturated, conditionally unstable flow over a two-dimensional mountain ridge were performed to investigate how the unsaturated moist Froude number (F_w) and the mountain height-to-width aspect ratio affect the propagation, the cloud type and the pattern and amount of rainfall of orographically induced precipitation systems. This was tested through a series of idealized simulations using the Advanced Research Weather Research and Forecast (WRF) model (ARW). The F_w and h/a were varied by changing the basic wind speed and the mountain half-width, respectively. In all simulations, the mountain height and thermodynamic sounding were fixed at h = 2 km and CAPE = 3000 J kg^{-1}.

Numerical experiments with the aspect ratio (or a) fixed and F_w (or U) varying demonstrated that flow shifts to a higher number regime as F_w (or U) increases. These results are consistent with the findings of Chu and Lin (2000) and Chen and Lin

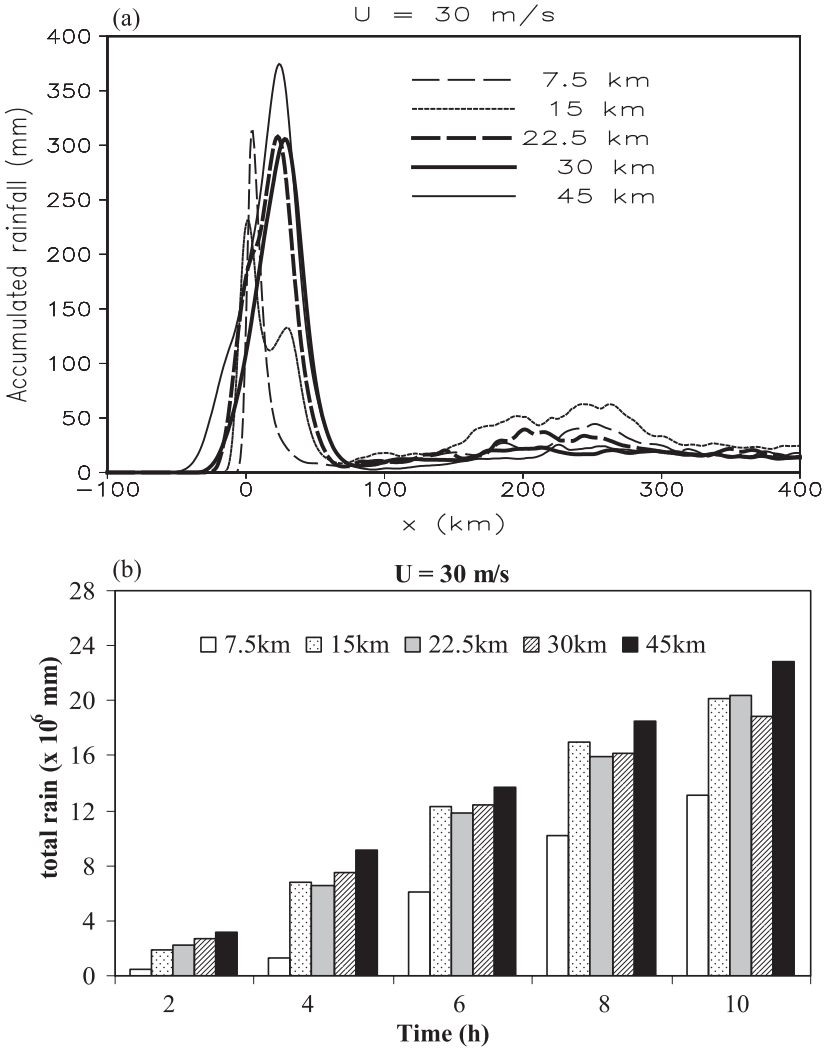

Fig. 9. (a) Spatial distribution of total accumulated rainfall (mm) after 10-h simulations and (b) accumulated total rainfall (mm) after 2-, 4-, 6-, 8-, and 10-h integration for a = 7.5, 15, 22.5, 30, and 45 km when U = 30 m s^{-1} (F_w = 1.572). The mountain height is 2 km.

(2005b). It was found that a slightly larger F_w is required for the regime transition to occur when the aspect ratio (mountain half-width) becomes smaller (larger). With a strong basic flow speed, such as U = 30 m s^{-1}, we also reproduced flow with an orographic stratiform precipitation system over the mountain and possibly a downstream propagating cloud system (i.e., Regime IV), as found in Chen and Lin (2005b).

On the basis of the flow regime definitions in Chen and Lin (2005b), we identified the flow regimes on the parameter space (h/a, F_w), which are shown in Table 1 and Fig. 11. Note that an additional set of experiments, which has a = 10 km (i.e., h/a = 0.2) and the same set of F_w, was performed and added into Fig. 11 to cover a more complete spectrum of the regime diagram. The regime diagram indicates that for low F_w, the flow belongs to an upstream propagating regime (i.e., Regime I) and is insensitive to h/a. For large F_w, both F_w and h/a dictate the precipitation pattern and the nature of the convection. When F_w is fixed, the flow shifts toward a downstream propagating regime with increasing h/a. This dependence on h/a for larger wind speeds appears to be linked to τ_{adv} and τ_{cloud}. It was also found that for the conditionally unstable flow studied here, although the local maximum rainfall is not directly correlated to F_w, the domain

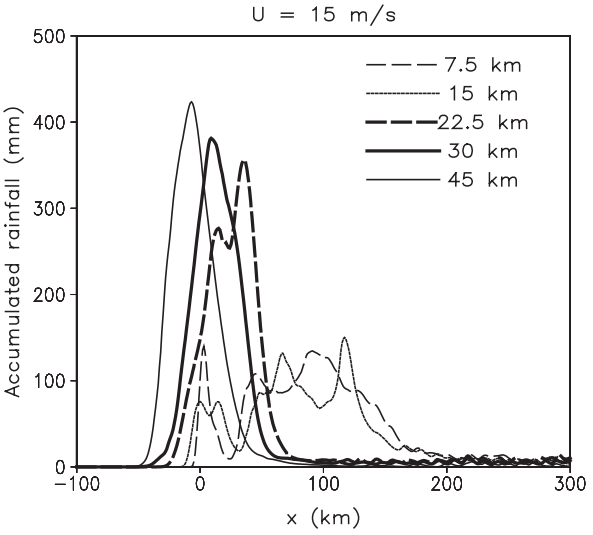

Fig. 10. Spatial distributions of total accumulated rainfall (mm) after 10-h simulations for a = 7.5, 15, 22.5, 30, and 45 km. The basic flow speed is U = 15 m s^{-1} (F_w = 0.786) and the mountain height is 2 km.

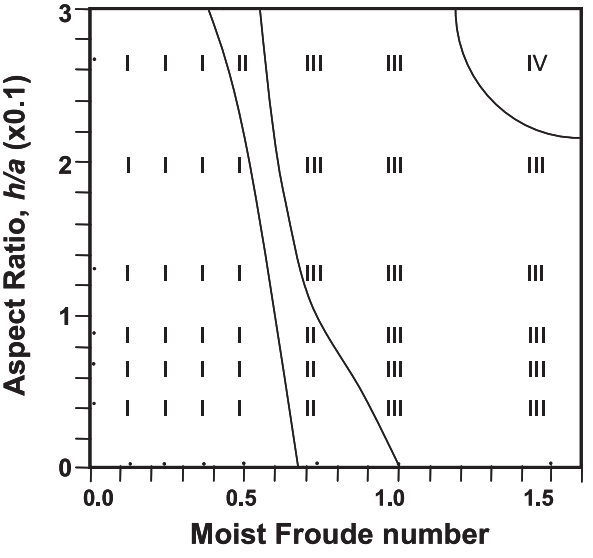

Fig. 11. Flow regime diagram on parameter space (F_w, h/a). In addition to experiments in Table 1, an additional set of runs, which has a = 10 km (i.e., h/a = 0.2) and the same set of F_w, was performed and added here to cover a more complete spectrum of the regime diagram.

integrated rainfall is sensitive to basic wind speed, in particular for those low number flow regimes (i.e., weak basic winds) when h/a is fixed. On the other hand, the domain integrated accumulated rainfall is not sensitive to h/a when F_w is fixed. A sounding with a large CAPE was used in this study. However, it is expected that when the CAPE of the sounding becomes smaller (i.e., with other parameters, such as F_w and a, fixed), the flow can be shifted to a larger flow regime, as discussed in Chen and Lin (2005b).

In the relationship between rainfall patterns and flow regimes, it was found that flash floods may occur over mountain areas when 1) quasi-stationary convective precipitation systems stay over the mountain region for a significant period of time (i.e., Regime II); or 2) abundant moisture is supplied into the precipitation systems over the mountain region for a significant period of time for flow Regimes III and IV. It was also found that local orographic rainfall from stratiform precipitation systems which belong to Regime IV can be as heavy as that from convective or mixed type precipitation systems which belong to Regime III. It is important to keep in mind that flash floods can also happen in the foothills of the mountains, where the direct rainfall is low but surface water runoff is large.

Acknowledgments

The authors would like to acknowledge the WRF model development team for their efforts in developing this model. Contribution from Heather Reeves on an earlier version of this work is acknowledged. This research is supported by NSF Grant ATM-0344237.

References

Chen, S.-H. and Y.-L. Lin, 2005a: Orographic effects on a conditionally unstable flow over an idealized three-dimensional mesoscale mountain. *Meteor. Atmos. Phys.*, **88**, 1–21.

Chen, S.-H. and Y.-L. Lin, 2005b (CL05): Effects of moist Froude number and CAPE on a conditionally unstable flow over a mesoscale mountain ridge. *J. Atmos. Sci.*, **62**, 331–350.

Chen, S.-H. and W.-Y. Sun, 2002: A one-dimensional time-dependent cloud model. *J. Meteor. Soc. Japan*, **80**, 99–118.

Chu, C.-M. and Y.-L. Lin, 2000: Effects of orography on the generation and propagation of mesoscale convective systems in a two-dimensional condi-

tionally unstable flow. *J. Atmos. Sci*., **57**, 3817–3837.

Colle, B.A., 2004: Sensitivity of orographic precipitation to changing ambient conditions and terrain geometries: an idealized modeling perspective. *J. Atmos. Sci*., **61**, 588–606.

Jiang, Q., 2003: Moist dynamics and orographic precipitation. *Tellus*, **55A**, 301–316.

Kirshbaum, D.J. and D.R. Durran, 2004: Factors governing cellular convection in orographic precipitation. *J. Atmos. Sci*., **61**, 682–698.

Michalakes, J., S.-H. Chen, J. Dudhia, L. Hart, J. Klemp, J. Middlecoff, and W. Skamarock, 2001: Development of a next generation regional weather research and forecast model in Developments in Terracomputing. Proceedings of the Ninth ECMWF Workshop on the Use of High Performance Computing in Meteorology. Eds. Walter Zwieflhofer and Norbert Kreitz. World Scientific, Singapore. 269–276.

Miglietta, M.M. and A. Buzzi, 2004: A numerical study of moist stratified flow regimes over isolated topography. *Quart. J. Roy. Meteor. Soc*., **130**, 1749–1770.

Rauber, R.M., 1992: Microphysical structure and evolution of a Sierra Nevada shallow orographic cloud system. *J. Appl. Meteor*., **31**, 3–24.

Schlesinger, R.E., 1978: A three-dimensional numerical model of an isolated thunderstorm: Part I. Comparative experiments for variable ambient wind shear. *J. Atmos. Sci*., **35**, 690–713.

Sinclair, M.R., D.S. Wratt, R.D. Henderson, and W.R. Gray, 1997: Factors affecting the distribution and spillover of precipitation in the Southern Alps of New Zealand – A case study. *J. Appl. Meteor*., **36**, 428–442.

Skamarock, W.C., J.B. Klemp, J. Dudhia, D.O. Gill, D.M. Barker, W. Wang, and J.G. Powers, 2005: A description of the advanced research WRF version 2. NCAR technical note, 100 pp (also see http://www.mmm.ucar.edu/wrf/users/docs/arw_v2.pdf).

Smith, R.B., 1979: The influence of mountains on the atmosphere. *Advances in Geophys*., **21**, B. Saltzman (Ed.), Academic Press, 87–230.